10

FERMILAB
MAY 9 1998

ISAS-RN-647

Fermilab Library
0 1160 0061638 7

ISAS RESEARCH NOTE

ISAS RN 647

Where Are the X-Ray Event Grades Formed Inside the Pixel of the Charge-Coupled Device?

The Behavior of the Primary Charge Cloud Inside the CCD

Hiroshi Tsunemi, Junko Hiraga, Kumi Yoshita
and Shunji Kitamoto

NAME | DATE | M.G.

RETURN TO FERMILAB LIBRARY

THE INSTITUTE OF SPACE AND ASTRONAUTICAL SCIENCE

THE INSTITUTE OF SPACE AND ASTRONAUTICAL SCIENCE
YOSHINODAI, SAGAMIHARA, KANAGAWA 229-8510

ISAS RESEARCH NOTE

ISAS RN 647

Where Are the X-Ray Event Grades Formed Inside the Pixel of the Charge-Coupled Device ?

The Behavior of the Primary Charge Cloud Inside the CCD

Hiroshi Tsunemi[1,2,3], Junko Hiraga[1,2], Kumi Yoshita[1,2], and Shunji Kitamoto[1,2]

April 1998

[1] *Department of Earth and Space Science, Graduate School of Science, Osaka University*
1-1, Machikaneyama, Toyonaka, Osaka, 560-0043. Japan
[2] *CREST, Japan Science and Technology Corporation (JST)*
[3] *Institute of Space and Astronautical Science, 3-1-1 Yoshinodai, Sagamihara, Kanagawa 229-8510, Japan*
Inst. Space Astron. Sci.

To appear in Jpn. J. Appl. Phys., vol. 37, No.5, part 1

Where Are the X-Ray Event Grades Formed Inside the Pixel of the Charge-Coupled Device ? The Behavior of the Primary Charge Cloud Inside the Charge-Coupled Device.

Hiroshi TSUNEMI [1,2], *Junko HIRAGA [1,2], Kumi YOSHITA [1,2] and Shunji KITAMOTO [1,2]
[1]Department of Earth and Space Science,Graduate School of Science, Osaka University,
1-1 Machikaneyama-cho, Toyonaka, Osaka 560-0043, Japan
[2]CREST, Japan Science and Technology Corporation (JST)

ABSTRACT

We report the use of an improved technique to measure the X-ray detection efficiency of a charge-coupled device (CCD) with a subpixel resolution. This technique makes use of a parallel X-ray beam and metal mesh placed closely on the CCD. The mesh has many circular holes spaced at distance of 4 times the CCD pixel size (multi-pitch mesh). We could identify the interaction position of X-rays both for single events and for split pixel events. By using this method, we demonstrated how various types of X-ray events are formed inside the CCD. We have already shown that the two-pixel split events were formed near the pixel boundary. We clearly showed that the three-pixel events were formed when the interaction position was close to the pixel corner ,whereas the four-pixel split events were formed when the interaction position was much closer to the pixel corner. We found that the center of gravity of split events could represent the interaction position with an uncertainty of 0.13 pixel size.

KEY WORDS: charge-coupled device, X-ray event, split event, subpixel resolution

1. Introduction

A charge-coupled device (CCD) is now widely used as an X-ray photon count detector, particularly in astronomy.[1, 2] When we reduce the incident X-ray flux such that the primary electron clouds produced by the X-ray photon do not overlap with each other, we can obtain the X-ray energy spectrum as well as the X-ray image.

Recently, we introduced a new technique to obtain the X-ray response of the CCD with a subpixel resolution.[3] The new technique consists of a metal mesh closely placed on the CCD and a parallel X-ray beam. The mesh has a large number of small holes with periodic spacing, equal to that of the CCD pixel size. We call this a 'single-pitch mesh'. We could restrict the input X-ray position with a subpixel resolution which enables us to study the X-ray response in detail.[4, 5] The latest technique is to employ a mesh whose hole spacing is a multiple of the CCD pixel size, which we call a 'multi-pitch mesh'. This enables us to restrict the interaction position of various types of X-rays in detail. This paper describes the advantageous points of this newer technique.

2. X-ray Event Grade

When the X-ray photon is photo-absorbed in the CCD, a primary charge cloud is formed. If the interaction occurs under the depletion region, it will diffuse out in all directions. Some of the charges moving backward will be lost in the substrate of the device. Those moving forward will be collected into the potential well when they reach the depletion layer. Even in this case, the

detected signal is that of a widespread multipixel cloud. Furthermore, the total charge collected in the potential well is not proportional to the incident X-ray energy.

If the interaction occurs in the depletion layer, the entire charge cloud will be collected in the potential well which is formed by the gates. We can read out the entire charge through the readout node. The output signal is proportional to the energy of the incident X-ray. The primary cloud size is relatively small in the energy range below 10 keV.[6] However, the entire charge cloud is not always collected in one pixel. There are several patterns of how the charge splits into neighboring pixels. In the ASCA SIS (the CCD camera on board the fourth Japanese X-ray astronomy satellite[7]), they employed 8 grades based on the patterns. When the primary charge is collected within one pixel (this is called a single event and 'grade 0'), the output of that pixel represents the incident X-ray energy. If the X-ray interaction position is close to the pixel boundary, the charge cloud will split into adjacent pixels and form a 'split event'. When the charge splits into vertically adjacent pixels, it is called a vertically split event and 'grade 2'. If the charge splits into horizontally adjacent pixels, it is called a horizontally split event and 'grade 3' or 'grade 4'. If the interaction position is close to the pixel corner, it will form 3- or 4-pixel event (called 'grade 6').

The new technique was invented[3] using a metal mesh placed just in front of the CCD which enabled us to confine the X-ray interaction position with a subpixel resolution. It was seen, for the first time, that the single events were formed only when the interaction position was well separated from the pixel boundary such that the whole primary charge was collected into one pixel. The following results were reported elsewhere.[4, 5] These results were obtained using a 'single-pitch mesh' which had a hole spacing equal to the CCD pixel size.

Figure 1(a) shows a schematic view of the experiment for a single-pitch mesh. The metal mesh with periodically spaced holes is placed on the CCD surface. The mesh is placed parallel to the CCD surface and tilted by a small angle, θ, against the pixel axis. The parallel X-ray beam is irradiated normal to the CCD surface. The X-rays passing through mesh holes reach the CCD. The X-ray interaction position is restricted by the mesh hole. The X-ray event, whose interaction position is far away from the pixel boundary, should take place in the pixel where a mesh hole sits in the center. This situation mainly generates single events. Whereas, the X-ray event, whose interaction position is

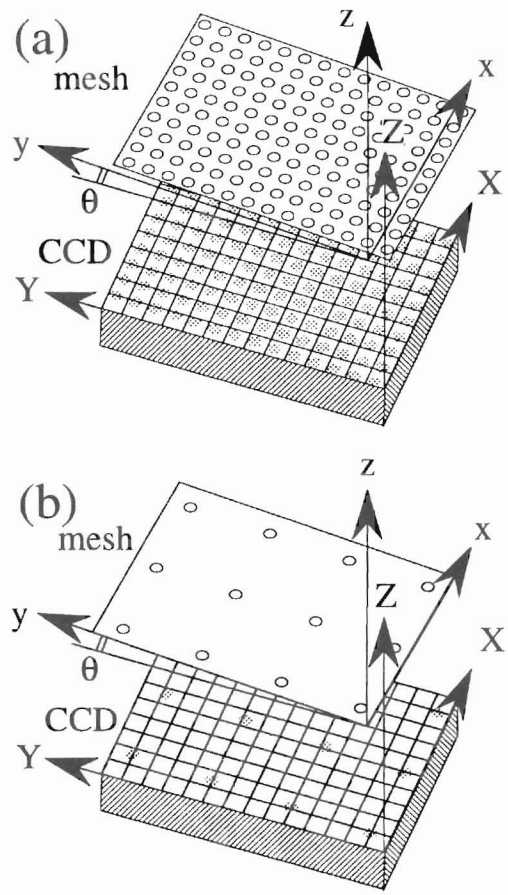

Fig. 1. A schematic view of the experiment. The hole shadow is represented by the hatched area. (a) A single-pitch mesh: the mesh hole pitch is equal to that of the CCD pixel size. (b) A multi-pitch mesh: the mesh hole pitch is four times larger than that of the CCD pixel size.

close to the pixel boundary, takes place in the pixel which has more than two hole shadows. This generates split events. This is inevitable for the single-pitch mesh since the hole has a finite size while its spacing is equal to the pixel size. Therefore, when we obtain the X-ray event pixel, we can not always uniquely determine the hole through which the X-ray enters.

To resolve the above problem, we introduced an improved mesh experiment using a 'multi-pitch mesh' whose hole spacing was a multiple of the CCD pixel spacing. Figure 1(b) shows a schematic view of the experiment for a hole spacing four times the CCD pixel size. We see that no pixel has more than 2 hole shadows because of a large spacing. We should note that there are many pixels which have no hole on them.

3. Experimental Setup

The copper metal mesh we used in the experiment is 10-μm-thick having holes of 3.4-μm diameter spaced at 48-μm. We designed the mesh holder such that it was placed 1 mm above the CCD surface. The mesh was tilted by about $-1°$ from the pixel direction so that we could obtain a moire pattern. We employed the same 21-m long X-ray beam line as employed in the previous experiment.[3] A 400-μm-thick beryllium window was replaced with a 15-μm-thick aluminum foil in order to improve the S/N of Al-K X-rays (1.5 keV). The applied voltage to the X-ray generator, the UltraX-18 (RIGAKU), was about 5 kV. The X-ray intensity was controlled such that the pileup did not introduce a serious problem. Figure 2 shows the obtained X-ray spectrum.

The transmission of 10-μm-thick copper foil is 10^{-3} at 3 keV and lower at lower X-ray energies. Therefore, we can say that the X-ray continuum above 3 keV penetrates the copper foil while all the Al-K X-rays reach the CCD through the mesh hole. Therefore, we can pick up the X-ray events through the mesh hole by selecting the Al-K X-rays.

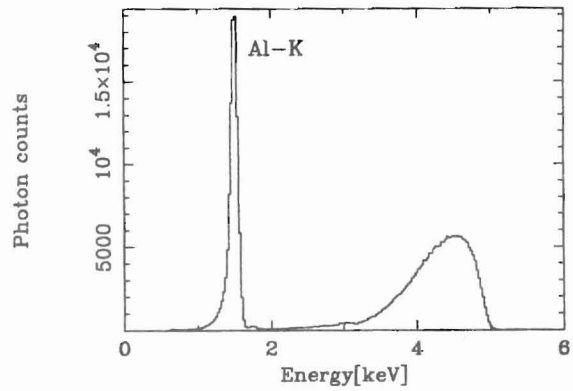

Fig. 2. The X-ray spectrum obtained with the CCD in the mesh experiment. The continuum above 3 keV comes from the X-rays penetrating the copper foil while Al-K X-rays come from those passing through the hole.

We employed a CCD chip, N11-5-5A0N-2, (Hamamatsu Photonics) of $12\,\mu m^2$ pixel size. The CCD chip was cooled down to $-60°$C. The CCD camera system was equipped with a mechanical shutter (60-μm-thick stainless steel) to block the Al-K X-rays. Our system can record images every 20 s (including the data transfer time to the hard disk of a computer). We selected an exposure time of about 5 s to maximize the number of isolated X-ray photons detected by the CCD. In this way, we operated the system for about 20 h, obtaining about 1×10^5 single events of Al-K X-rays.

4. Data Restoration Method

Figure 3 shows the distribution of the single events of Al-K X-rays obtained using a mesh with hole spacing of four times the pixel size. This is quite different from that obtained using the single-pitch mesh. Single events appear roughly at every 4×4 pixels due to the multi-pitch mesh.

In the single-pitch mesh experiment, a moire pattern itself is a direct expansion of the pixel image. Therefore, the pixel image with sub-pixel resolution can be obtained by analyzing the moire image[4] if the moire pattern size is big

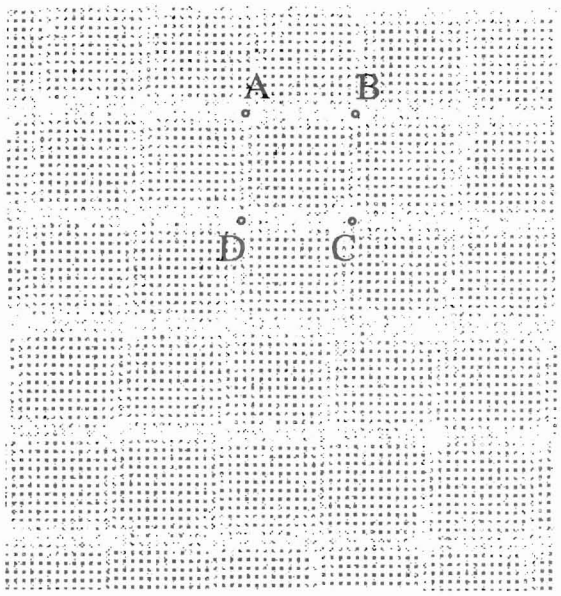

Fig. 3. A part of the raw image (250×250 pixels) obtained using single events is shown. Due to the multi-pitch mesh, most of the X-rays appear roughly at every 4×4 pixel.

enough and the X-ray beam intensity is uniform over the moire pattern. We employed a universal method[3, 5] which would function well even if the moire pattern was too small to be noticed.

In the present experimental setup, the moire pattern does not directly represent the pixel image. In the previous experiments using a single-pitch mesh, we assumed that the CCD pixel had a perfect square shape and that the distributed mesh holes were perfectly spaced. In this paper, the possible distortion effect of the mesh hole distribution is taken into account. The restoration method is described in detail in the following.

The CCD pixel coordinate, $\mathbf{X}$, is expressed in eq. (1) as

$$\mathbf{X} = C \begin{pmatrix} 1+a & 0 \\ 0 & 1+b \end{pmatrix} \begin{pmatrix} \cos\theta & -\sin\theta \\ \sin\theta & \cos\theta \end{pmatrix} \times \mathbf{x} + \mathbf{X_{off}}, \quad (1)$$

where $\mathbf{x}$ denotes the mesh hole coordinate, C is a coefficient of the multi-pitch mesh (it is 4 in our experiment), a and b are expansion coefficients on the mesh hole coordinate, θ is the tilt angle and $\mathbf{X_{off}}$ is an offset. These are several reasons due to which the expansion coefficients to be introduced. There are the X-ray beam divergence, the difference between the thermal contraction of the mesh and that of the CCD, the production accuracy of the mesh and the alignment of the mesh holder. a and b ($a \sim 0, b \sim 0$) are introduced in order to take into account the possible differences in mesh hole spacing on the CCD pixel coordinate.

The output of the nth pixel of the CCD, D_n, is expressed below as

$$D_n = \int_{nth\ pixel} M(\mathbf{x}) E(\mathbf{X}) d\mathbf{X}, \quad (2)$$

where $M(\mathbf{x})$ denotes the transmission of the mesh, and $E(\mathbf{X})$ is the detection efficiency of the CCD.

The transmission of the mesh is expressed by eq. (3) as

$$M(\mathbf{x}) = \int H(\mathbf{x}') L(\mathbf{x} - \mathbf{x}') d\mathbf{x}', \quad (3)$$

$$H(\mathbf{x}) = \begin{cases} 1 & (\ |\mathbf{x}| < r) \\ \textit{metal} \\ \text{transmission} & \sim 0 \quad (\ |\mathbf{x}| > r\ ) \end{cases} \quad (4)$$

where $H(\mathbf{x})$ is the typical hole shape of the mesh, $L(\mathbf{x})$ denotes the hole position on the mesh and r is the radius of the effective hole size. In our experimental setup, r is about $2\,\mu$m taking into account the diffraction of Al-K X-rays. Since the hole is periodically spaced, we obtain

$$L(\mathbf{x}) = \sum_{\mathbf{n}=integer\ lattice} \delta(\mathbf{x} - \mathbf{n}) \quad . \quad (5)$$

Once we assume some values for a, b, θ and $\mathbf{X_{off}}$, we can restore a pixel image. The precise values for these parameters can be obtained by searching a set of values which produce the largest variance in the restored image.[3] In the single-pitch mesh, $\mathbf{X_{off}}$ does not play an important role since it only affects the simple offset in the restored image. This is due to the fact that each pixel has its corresponding mesh hole as shown in Fig. 1(a). In the multi-pitch mesh, in

contrast, there are many pixels having no mesh hole on them as shown in Fig. 1(b). Therefore, even if we pick up the true values for a, b and θ, we have to identify the true value for $\mathbf{X_{off}}$ so that the restored image is constructed using pixels corresponding to the mesh holes.

From the practical point of view, it is a rather complicated problem to identify a set of true values for the parameters. Furthermore, there are many alias values[8] producing a similar moire pattern. Next, we describe how we can obtain a, b, θ and $\mathbf{X_{off}}$ from the image.

We can precisely measure $\mathbf{X}$ whereas we cannot measure $\mathbf{x}$. Yoshita et al.[5] described a method for the single-pitch mesh with the assumption of $a = b$. Firstly, we estimate rough values for the parameters. Figure 3 shows a grid pattern; let ABCD represent one element of that moire pattern. Let $\overrightarrow{\mathrm{AB}}$ be represented by $\mathbf{X}$ on the CCD coordinate and by $\mathbf{x}$ on the mesh coordinate, respectively. Then we obtain $(1+a)^2 = (X^2+Y^2)/(x^2+y^2)$ and $\tan\theta = (Yx - Xy)/(Xx + Yy)$. Since $\overrightarrow{\mathrm{AB}}$ denotes one element of the moire pattern, we can expect the following to hold:

$$\begin{aligned} \mathbf{X} - \mathbf{x} &= \begin{pmatrix} X \\ Y \end{pmatrix} - \begin{pmatrix} x \\ y \end{pmatrix} \\ &= \begin{pmatrix} \pm 1 \\ 0 \end{pmatrix} or \begin{pmatrix} 0 \\ \pm 1 \end{pmatrix}. \end{aligned} \tag{6}$$

In total, given the assumptions $a, \theta \sim 0$, which are true in our experiment, there are four possibilities. These are:

$$\begin{aligned} (a,\theta) \approx\ & \left(\tfrac{\pm X}{X^2+Y^2}, \tfrac{\mp Y}{X^2+Y^2}\right), or \\ & \left(\tfrac{\mp Y}{X^2+Y^2}, \tfrac{\pm X}{X^2+Y^2}\right) \end{aligned} \tag{7}$$

Similarly, we obtain the same relationship for (b,θ) by letting $\overrightarrow{\mathrm{AD}}$ be represented by $\mathbf{X}$ and $\mathbf{x}$.

The values of a and b are unknown whereas the value of θ is known. Once we assumed some values for a, b, θ and $\mathbf{X_{off}}$, we could restore the pixel image. The precise values for these parameters are obtained by searching for the values which produce the largest variance in the restored image. From the data shown in Fig. 3, we obtain as follows.

$$\mathbf{X_{AB}} = \begin{pmatrix} 50.9 \\ -0.7 \end{pmatrix} and\ \mathbf{X_{AD}} = \begin{pmatrix} -4.4 \\ -50.3 \end{pmatrix}. \tag{8}$$

We set θ at around $-1°$. In the experimental setup, the mesh temperature was expected to be almost equal to that of the CCD. Therefore, we expect $a, b \sim -1 \times 10^{-3}$, taking into account both the beam divergence and the thermal contraction. Therefore, we searched a region in the a, b, θ values surrounding $a = -1 \times 10^{-3}$, $b = -1 \times 10^{-3}$ and $\theta = -1°$ for the image with maximum variance. Even if we assume some values for them, we have to identify the true value of $\mathbf{X_{off}}$ ($0 \le X_{off}, Y_{off} \le 4$ in our case). We select $\mathbf{X_{off}}$ such that we maximize the number of X-ray events contributing to the image restoration. In this way, the image variance was maximized at $a = -0.5 \times 10^{-3}$, $b = -1.3 \times 10^{-3}$, $\theta = -1.15°$, $X_{off} = 2.05$ and $Y_{off} = 0.55$. We have adopted these values for the restored images presented in the remainder of this paper. We notice that a is different from b. It implies that either the hole mesh spacing or the CCD pixel spacing along the x axis is longer by 0.8×10^{-3} than that along the y axis. Our results do not depend on the actual specific case.

5. Data Analysis

5.1. Restoration of images for various types of X-ray events

So far, we employed the method to select the X-ray events which was used in the ASCA satellite. First of all, we pick up the pixel whose output is above the event threshold, T_{event}. If the pixel output is above T_{event} and is the local maximum (its output is larger than those of adjacent pixels), the pixel is called the 'X-ray pixel'. The X-ray pixel is considered to be the interaction position of the X-ray. We selected X-ray events according to the number of pixels exceeding a particular 'split threshold', T_{split}. Some examples are schematically shown in Fig. 4.

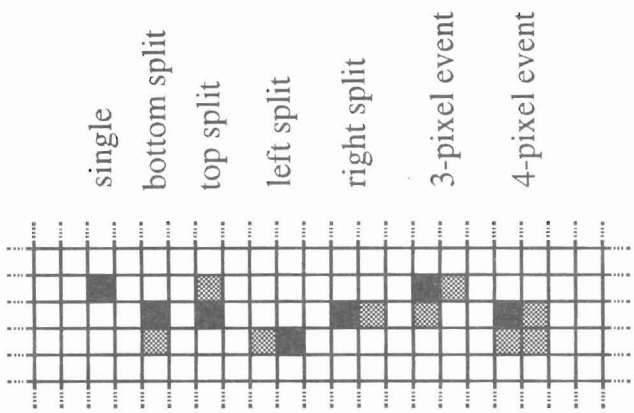

Fig. 4. Some examples of the X-ray event patterns produced on the CCD. Each small square represents the CCD pixel. The black pixels represent the 'event pixel' which is higher than T_{event} and is the local maximum. The hatched pixels represent the 'split pixel' which is higher than T_{split}. From left to right, these are 'single event', 'bottom split', 'top split', 'left split', 'right split', '3-pixel event', '4-pixel event'. There are four types of 3- and 4-pixel events. Among them, we only display the events whose event pixels are in the left top part of the X-ray pattern.

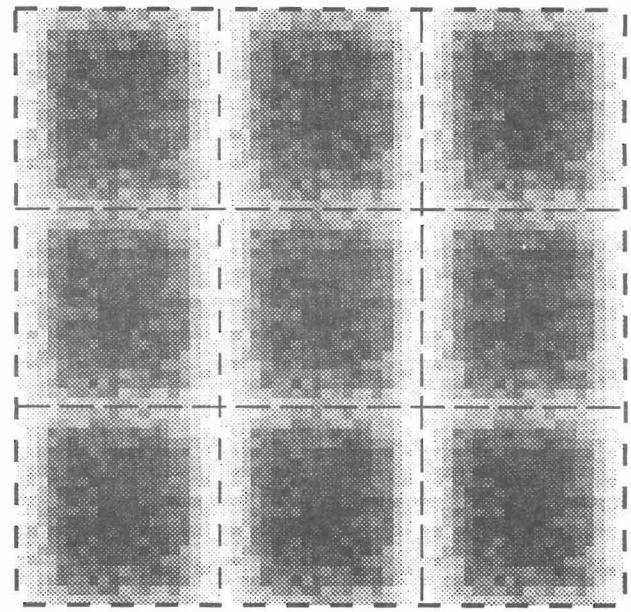

Fig. 5. The X-ray intensity maps for single events with subpixel resolution of 3×3 pixels are shown. Pixel boundary is shown as a dashed line.

As shown in Fig. 5, we obtained a restored image of the 'representative pixel (RP)' using single events. We reproduced 3×3 RP in the figure. The pixel boundary is indicated by a dashed line. This clearly shows that the single events occur when the interaction position of the X-ray is well separated from the pixel boundary.[3, 4, 5] The dark region represents the convolution of the effective hole size and the region where the X-rays form single events. The width of the boundary region where no single event occurs depends both on the primary charge size and on the mesh hole size.

Next, we divide two-pixel events according to their pattern. In two-pixel events, there are two adjacent pixels whose outputs are above T_{split}. We call the higher output pixel the event pixel, while the lower output pixel is the split pixel. Therefore, there are four shapes according to the position of the split pixel shown in Fig. 4: a left split event, a right split event, a top split event and a bottom split event. We restore the RP for them. Figure 6 show RPs for four types of two-pixel events. We can clearly see the difference between them. The right split events occur when the X-ray enters the right boundary portion of the pixel where the primary charge easily splits onto the adjacent right pixel. Whereas, the left split events occur when the X-ray enters the left boundary portion of the pixel. We also see similar results for vertically split two-pixel events.

Similarly, we divide 3- or 4-pixel events according to their pattern in detail. As can be easily seen, the 3- or 4-pixel events occur when the X-rays enter the corner portion of the pixel. Figures 7(a) and 7(b) show RP for 3-pixel events and for 4-pixel events, respectively. We observed four types of 3- or 4-pixel events when we displayed the events whose event pixel was in the left top part of the X-ray pattern. Other three types show quite similar images. This figure clearly shows that the primary charge splits into the diagonal pixel when the X-rays enter very close to the corner of the pixel. We should note that we can divide the events in more detail than in the previous works.[4, 5] This is one of the advantages of the multi-pitch mesh experiment which cannot be exhibited by a single-pitch mesh

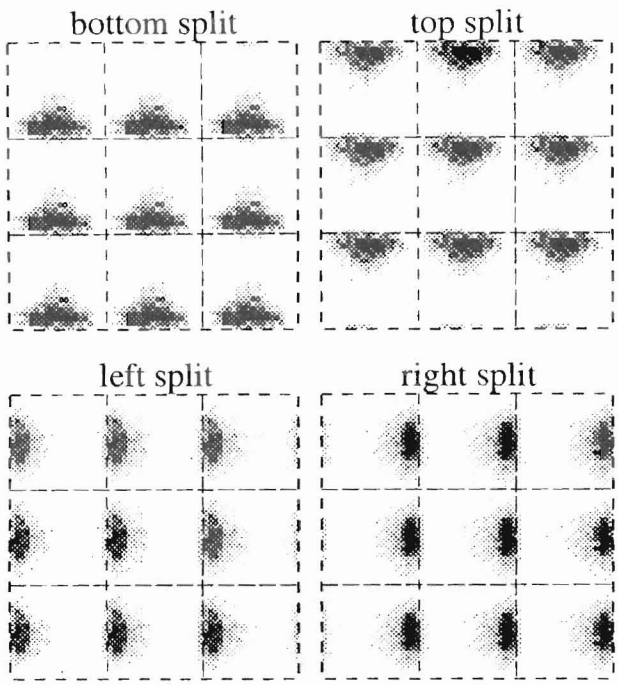

Fig. 6. Same as that for Fig.5 but for split two-pixel events.

experiment.

5.2. Specification of the interaction position of X-rays

Since we use the multi-pitch mesh, we can unambiguously specify the interaction position of X-rays. So far, the local maximum pixel (event pixel) has been considered as the interaction position of X-rays. We can measure the distance between the event pixel and the true interaction position (hole position). Figure 8 shows the event distribution, D_{event}, according to the distance between the event pixel location and the true interaction position, by means of solid lines. This figure shows an uncertainty when we consider the event pixel location as the interaction position of the X-ray.

For single events, the uncertainties of D_{event} are smaller than 0.5 pixel size. This means that the single event must occur at the pixel in which the X-ray enters. Whereas, the uncertainties of D_{event} for two-pixel split events have two peaks indicating larger uncertainties than those of single events. When the X-ray enters near the pixel boundary, the charge will evenly split into two

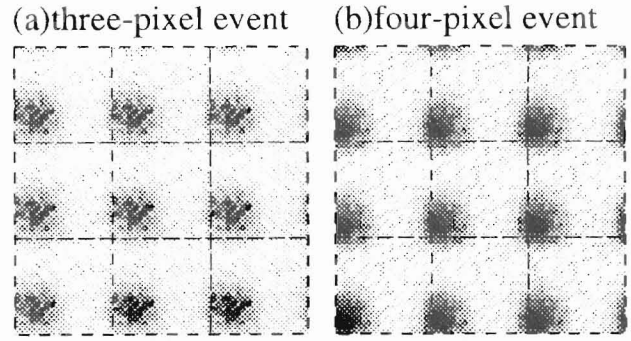

Fig. 7. Same as that for Fig.5 but (a) for 3-pixel events and (b) for 4-pixel events. This figure only shows the data for events displayed in Fig.4.

pixels. Then, the event pixel does not show the X-ray interaction position precisely. Therefore, we can consider the event pixel representing the X-ray interaction position for single events while we cannot for split events.

We introduced a center of gravity, $\mathbf{X_c}$, of the event to determine the interaction position from the event pattern. We can calculate the $\mathbf{X_c}$ weighting by means of the signal output of the pixels in eq. (9) as

$$\mathbf{X_c} = \frac{\sum D_n \mathbf{X_n}}{\sum D_n}, \tag{9}$$

where $\mathbf{X_n}$ represents the nth pixel position.

Figure 8 also shows the event distribution, D_{cg}, according to the distance between the center of gravity of the event and the true interaction position by means of dashed lines. We observe D_{cg} to be identical to D_{event} for single events while we don't for split events. By taking into account the uncertainty of the interaction position for single events, we can say that the single event occurs at the pixel where the X-ray enters. In the two-pixel events, we see much finer distribution for D_{cg} than that for D_{event}. When we fit it for D_{cg} using a single Gaussian function, we obtain 0.13 pixel size as $1\,\sigma$. By using the split events, we can specify the interaction position of X-rays with a subpixel resolution.

These results clearly show that the center of gravity gives a better interaction position than

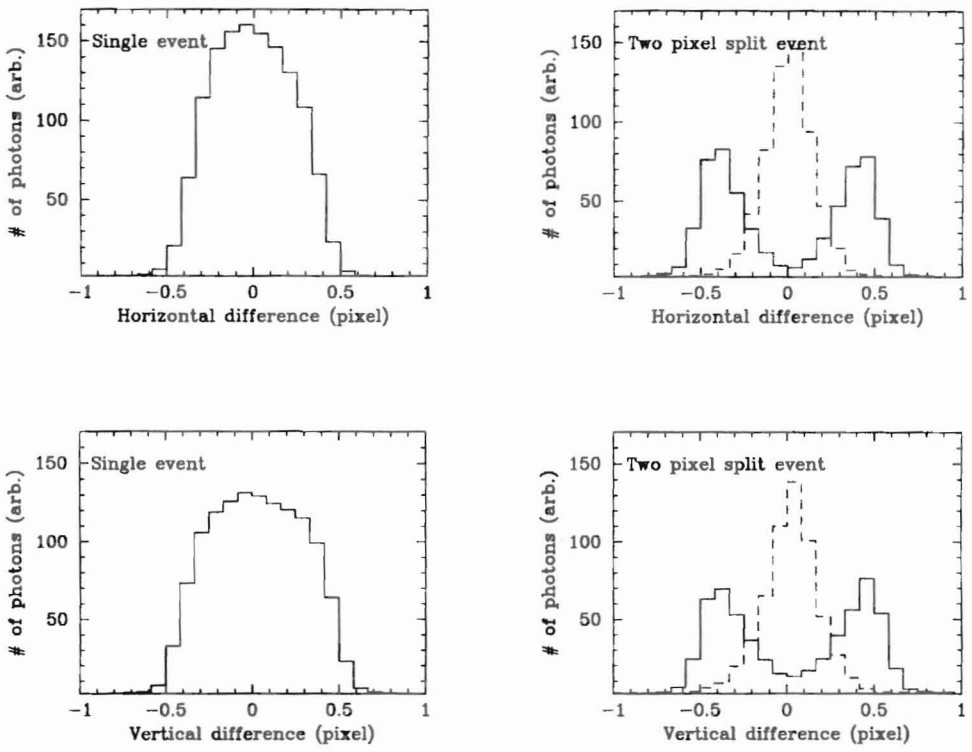

Fig. 8. Position uncertainties of single events are shown along the X-axis (top left) and along the Y-axis (bottom left). Those of split events are shown along the X-axis (top right) and along the Y-axis (bottom right). The solid line represents the distribution of D_{event} while the dashed line represents the distribution of D_{cg}. For single events, D_{event} is identical to D_{cg}.

the event pixel. The uncertainty is always better than 0.5 pixel size for any grade event by employing the center of gravity of the event as the interaction position while it is not by employing the event pixel as the interaction position. In the single-pitch mesh experiment, the distance to the nearest mesh hole from the event pixel location is always smaller than 0.5 pixel size.

So far, the event pixel was taken as the interaction position in the single-pitch mesh experiment.[4, 5] Therefore, the interaction position could not be uniquely specified except for the single events. As a result, the left split two-pixel events (grade 3) and the right split two-pixel events (grade 4) were combined. If the method to determine the interaction position of X-rays using the center of gravity is employed instead of the event pixel, the interaction position can be uniquely determined.

6. Conclusion

We presented here an improved mesh experiment using a multi-pitch mesh. This technique unambiguously determined the X-ray interaction position inside a CCD pixel. This enables us to experimentally confirm that the event pixel coincides with the interaction position. The primary charge splits into the adjacent pixel only when the interaction position is close enough to the pixel boundary.

We introduced a new method to determine the interaction position of X-rays employing the center of gravity of the event. This method improved the determination accuracy of the interaction position of split events. The uncertainty of this method is only about 0.13 times the pixel size. Furthermore, we were able to determine the precise interaction position of the single event either by the event pixel or by the center of gravity.

Therefore, our new method enables us to determine the interaction position of X-rays not only for the multi-pitch mesh experiment but also for the single-pitch mesh experiment.

From the practical point of view, the single-pitch mesh experiment has an advantage that a moire pattern is a direct expansion of RP. However, it is impractical to fabricate various types of meshes to fit various kinds of CCD pixel sizes, since pixel sizes are different for different CCDs. If a mesh hole spacing is equal to or larger than the pixel size, we can unambiguously determine the interaction position of X-rays. Therefore, our mesh having holes spaced at 48-μm can be applied to any CCD whose pixel size is smaller than 48 μm. Even if we cannot obtain a moire pattern, we can restore RP by identifying true parameter values.

7. Acknowledgements

The authors express their special thanks to all the member of the CCD group in Osaka university. They also thank to Mr. K. Miyaguchi in Hamamatsu Photonics who supported this experiment from the technical point of view. KY is partially supported by JSPS Research Fellowship for Young Scientists, Japan. This work is partially supported by the Grants-in-aid by the Ministry of Education, Science and Culture of Japan (09640320).

Bibliography

[1] G. W. Frazer: *X-ray Detectors in Astronomy* (Cambridge University press, Cambridge, 1989) p. 208.

[2] B. E. Burke, R. W. Mountain, P. J. Daniels, M. J. Cooper and V. S. Dolat: IEEE Trans. Nucl. Sci. **41** (1994) 375.

[3] H. Tsunemi, K. Yoshita and S. Kitamoto, Jpn. J. Appl. Phys. **36** (1997) 2906.

[4] M. J. Pivovaroff, S. Jones, M. Bautz, S. Kissel, G. Prigozhin, G. Ricker, H. Tsunemi and E. Miyata: submitted to IEEE Trans. Nucl. Sci.

[5] K. Yoshita, H. Tsunemi, K. C. Gendreau, G. Pennington and M. W. Bautz: to be published in IEEE Trans. Nucl. Sci. **45** (1998).

[6] J. Janesick, T. Elliott and G. Garmire: Proc. SPIE **597** (1985) 364.

[7] Y. Tanaka, H. Inoue and S. S. Holt: Publ. Astron. Soc. Jpn. **46** (1994) 37.

[8] H. Tsunemi, K. Yoshita, S. Kitamoto, and E. Miyata: Proc. SPIE **3114** (1997) 230.